SICE Annual Conference 2014
September 9-12, 2014, Hokkaido University, Sapporo, Japan

Knee Constraint Effects of Bipedal Walking by Visual-lifting Approach

Hiroki Imanishi[1†], Mamoru Minami [1†] , Akira Yanou[1†] and
Jumpei Nishiguchi[1†]

[1]Graduate School of Natural Science and Technology, Okayama University, Okayama, Japan
(Tel: +81-86-251-8924; E-mail: minami-m@cc.okayama-u.ac.jp)

Abstract: Recently, a lot of biped robots are being investigated and developed. Although humans walk with their knees extending, humanoid robots walk with their knees bending. Walking with their knees bending has advantages that it is not needed to consider the complex models such as toe and heel, and the area of bottom of foot can increase to keep walking stable. However, walking with knees extending can reduce energy and be closed to natural walking. Moreover, length of stride can also increase when knee is full extended. Therefore, it is necessary to make humanoid robot with knee constraint to extend the knee in walking. In this paper, we make humanoid robot with human's knees structure which has a constraint of knee joint angle motion through simulation and investigated its influence to humanoid walking.

Keywords: knee constraint, humanoid robot.

1. INTRODUCTION

As for walking control of the humanoid robot, ZMP-based walking is known as the most potential approach, which has been proved to be a realistic control strategy to demonstrate stable walking of actual biped robots, since it can guarantee that the robots can keep standing by retaining the ZMP within the convex hull of supporting area [1], [2]. Instead of the ZMP, another approaches that put the importance on keeping the robot's walking trajectories inside of a basin of attraction [3]-[5] including a method referring limit cycle to determine input torque [6].

These previous discussions are based on simplified bipedal models, which tend to avoid discussing the effects of feet or slipping existing in real world. Contrarily to the above references, a research [7] has pointed out that the effect of foot bears varieties of the walking gait, e.g., point contacting (heel contacting) and surface contacting (foot sole contacting with ground), causing changing of dimension of state variables. Our research has begun from such view point of [7] as aiming at describing gait's dynamics as correctly as possible, including point/surface-contacting state of foot, slipping of the foot and bumping, where walking gait states transfer based on the past walking motions, called event-driven. However, our model differs from [7] in the point that it uses leg model without body, arms and head, instead of that we discuss the dynamics of whole-body humanoid. And in what the authors think important is that the dimension of dynamical equation will change depending on the walking gaits' varieties, which introduced by [8] concerning one-legged hopping robot.

Given as an example that heel be detached from ground while its toe being contacting, a new state variable describing foot's rotation would emerge, resulting in an increase of a number of state variables. In fact, this kind of dynamics with the dimension number of state variables being changed by the result of its dynamical time profiles of motions are out of the area of control theory that discusses how to control a system with fixed states' number. Further the tipping over motion has been called as non-holonomic dynamics that includes a joint without inputting torque, i.e., free joint.

Meanwhile, landing of the heel or the toe of lifting leg in the air to the ground makes a geometrical contact. [9] mentioned how to represent contacting with environment that can handle constraint motion with friction by algebraic equation and applied it to human figures [10]. On the basis of these references, we derive dynamics of eleven kinds of gaits including slipping motion with both varying constraint conditions and changing of the dimension of state variables where the humanoid's dynamical model has been elaborated as much as possible.

When ZMP is to be on the edge of convex hull of foot, meaning the humanoid is in a state of toe-off, the gait deems to be unstable. In this paper, ZMP-independent walking is proposed to realize human-like natural walking including toe-off state, that is a method to enhance standing robustness named "Visual-lifting Approach" based on visual servoing and visual feedback concept, which is based on a similar concept of impedance control method [16]. Real-time pose tracking method is used for observing a static object that is set in front of the robot to measure the robot's head position/orientation based on the object through visual pose estimation [17], [18] during walking. The simulation results show that visual feedback helps realize stable bipedal walking that ZMP is not kept within convex hull of supporting area on condition that humanoid's dynamics includes toe-off, slipping and bumping.

Moreover, many humanoid robots don't stretch the leg like upright human walking. This walking achieves fewer burden on hip joint and uses in less energy because upright walking configuration can save energy for walking than non-upright one. And fashion models stretch legs vigorously while walking. Therefore, we estimate they try to lengthen the stride and make beautiful look. So we make humanoid simulation by knee constraint and inves-

† Hiroki Imanishi is the presenter of this paper.

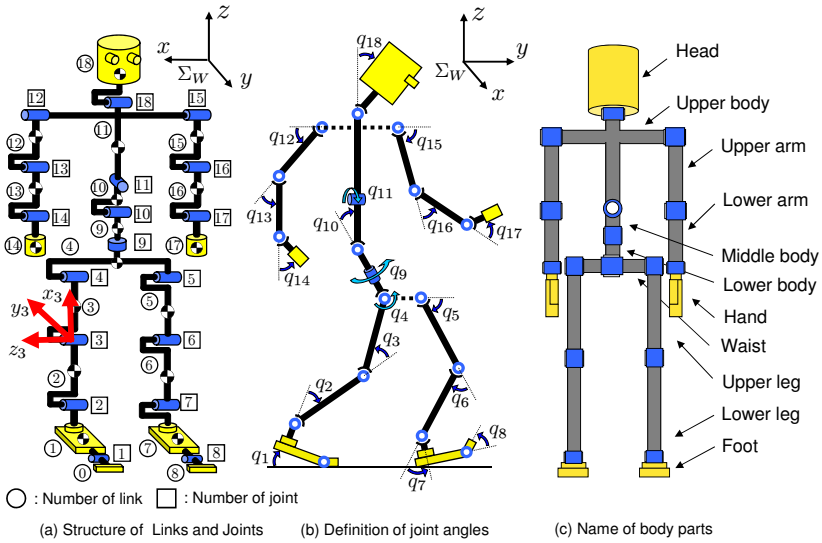

Fig. 1 Definition of humanoid's link, joint and angle number

Table 1 Physical parameters

Link	l_i	m_i	d_i
Head	0.24	4.5	0.5
Upper body	0.41	21.5	10.0
Middle body	0.1	2.0	10.0
Lower body	0.1	2.0	10.0
Upper arm	0.31	2.3	0.03
Lower arm	0.24	1.4	1.0
Hand	0.18	0.4	2.0
Waist	0.27	2.0	10.0
Upper leg	0.38	7.3	10.0
Lower leg	0.40	3.4	10.0
Foot	0.07	1.1	10.0
Total	1.7	63.8	

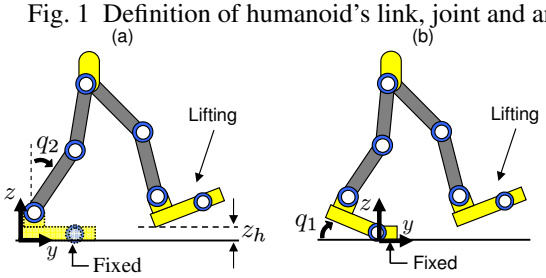

Fig. 2 Gaits including floating-foot

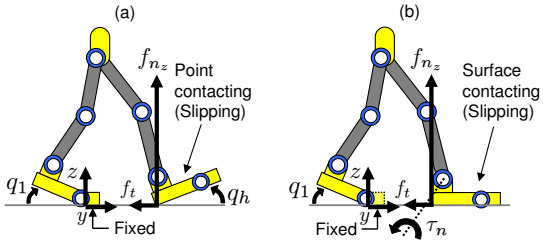

Fig. 3 Gaits including contacting-foot (Slipping)

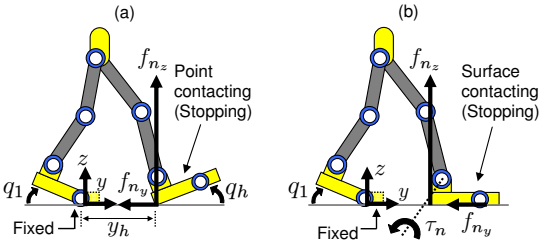

Fig. 4 Gaits including contacting-foot (No slipping)

tigate hip joint angle.

2. DYNAMICAL WALKING MODEL

We discuss a biped robot whose definition is depicted in Fig.1. Table 1 indicates length l_i [m], mass m_i [kg] of links and joints' coefficient of viscous friction d_i [N·m·s/rad], which are decided based on [11]. Our model represents rigid whole body— including feet, toe, torso, arms and body—having 18 degree-of-freedom. Detail explanation of this model is omitted, which is described in [19].

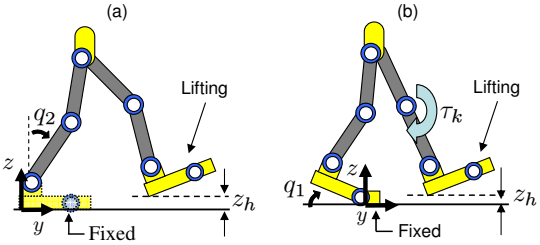

Fig. 5 Gaits including contacting-foot (Knee constraint)

2.1. Model with Contacting Constraints

Fig.2 dipicts two states with the lifting foot in the air. Giving that floating-foot contacts with a ground, two possible states like Fig.3 appear, where contacting-foot's position z_h or angle q_h to the ground are constrained. In Fig.3 (a) and (b), since the foot is constrained only vertical direction, foot's motion in walking direction (y-axis) has a degree of motion, that is, contacting-foot may slip forward or backward depending on the foot's velocity when contacting happens. Fig.5 (b) represents a situation that, a constraint condition restricting knee joint straight like human walking. When knee joint is constrained, q_6 (the knee joint angle of lifting leg) is set to be by 0[rad], this constraint condition is defined as C_4. Constraint torque τ_k is applied to knee of lifting leg in the direction of (b) during constrained motion. The constraints of foot's position , foot's rotation and knee joint angle are defined as C_1 , C_2 and C_4 respectively. These constraints are represented by Eq. (1), where Z_h means the contacting-foot's heel or toe position in Z-axis and q_h means sum the angle of foot is q_1+q_2+ ⋯ +q_7.

$$\boldsymbol{C}(\boldsymbol{r}(\boldsymbol{q})) = \begin{bmatrix} C_1(\boldsymbol{q}) \\ C_2(\boldsymbol{q}) \\ C_3(\boldsymbol{q}) \\ C_4(\boldsymbol{q}) \end{bmatrix} = \begin{bmatrix} Z_h(\boldsymbol{q}) \\ q_h(\boldsymbol{q}) \\ \dot{y}_h(\boldsymbol{q}) \\ q_6(\boldsymbol{q}) \end{bmatrix} = \boldsymbol{0} \qquad (1)$$

Here, C_3 is the constraint that contacting-foot does not slip (y_h is constant) as shown in Fig.4, which appears when velocity of the foot in walking direction $\dot{y}_h$ becomes less than small constant value ε in case of $|\dot{y}_h| < \varepsilon$,

meaning dynamic friction changes to static friction. On the other hand, C_3 disappears when contacting-foot's force in walking direction f_y exceeds static friction force f_t in case of $|f_y| > |f_t|$, meaning static friction changes to dynamic friction and slipping begins. Then, robot's equation of motion with external force f_{n_z}, f_{n_y}, friction force f_t, external torque τ_n and Constraint torque τ_k corresponding to C_1, C_2, C_3 and C_4 can be derived as follows:

$$\boldsymbol{M}(\boldsymbol{q})\ddot{\boldsymbol{q}} + \boldsymbol{h}(\boldsymbol{q}, \dot{\boldsymbol{q}}) + \boldsymbol{g}(\boldsymbol{q}) + \boldsymbol{D}\dot{\boldsymbol{q}} = \boldsymbol{\tau} + \boldsymbol{j}_{\mathrm{cz}}^{\mathrm{T}} f_{\mathrm{n_z}} - \boldsymbol{j}_{\mathrm{t}}^{\mathrm{T}} f_{\mathrm{t}} + \boldsymbol{j}_{\mathrm{r}}^{\mathrm{T}} \tau_{\mathrm{n}} + \boldsymbol{j}_{\mathrm{cy}}^{\mathrm{T}} f_{\mathrm{n_y}} + \boldsymbol{j}_{k}^{T} \tau_k \quad (2)$$

where $\boldsymbol{j}_{cz}$, $\boldsymbol{j}_t$, $\boldsymbol{j}_r$,$\boldsymbol{j}_{cy}$ and $\boldsymbol{j}_k$ are defined as:

$$\boldsymbol{j}_{cz}^T = \left(\frac{\partial C_1}{\partial \boldsymbol{q}^T}\right)^T \left(1/\left\|\frac{\partial C_1}{\partial \boldsymbol{r}^T}\right\|\right), \quad \boldsymbol{j}_t^T = \left(\frac{\partial \boldsymbol{r_n}}{\partial \boldsymbol{q}^T}\right)^T \frac{\dot{\boldsymbol{r_n}}}{\|\dot{\boldsymbol{r_n}}\|},$$
$$\boldsymbol{j}_r^T = \left(\frac{\partial C_2}{\partial \boldsymbol{q}^T}\right)^T \left(1/\left\|\frac{\partial C_2}{\partial \boldsymbol{q}^T}\right\|\right), \quad \boldsymbol{j}_{cy}^T = \left(\frac{\partial C_3}{\partial \boldsymbol{q}^T}\right)^T \left(1/\left\|\frac{\partial C_3}{\partial \boldsymbol{r}^T}\right\|\right)$$
$$\boldsymbol{j}_k^T = \left(\frac{\partial C_4}{\partial \boldsymbol{q}^T}\right)^T \left(1/\left\|\frac{\partial C_4}{\partial \boldsymbol{r}^T}\right\|\right)$$

It is common sense that (i) f_{n_z} (constraint force normal to floor) and f_t (friction force tangential to floor surface) are orthogonal, and (ii) value of f_t depends on f_{n_z} as $f_t = K f_{n_z}$ (K is constant scalar: $0 < K \leq 1$).

Moreover, differentiating Eq. (1) by time two times, then we can derive the constraint condition of $\ddot{\boldsymbol{q}}$.

$$\left(\frac{\partial C_i}{\partial \boldsymbol{q}^T}\right)\ddot{\boldsymbol{q}} + \dot{\boldsymbol{q}}^T \left\{\frac{\partial}{\partial \boldsymbol{q}}\left(\frac{\partial C_i}{\partial \boldsymbol{q}^T}\right)\right\}\dot{\boldsymbol{q}} + \boldsymbol{j}_k^T \tau_k = 0 \quad (i = 1, 2, 3, 4) \quad (3)$$

3. WALKING GAIT TRANSITION

Figure 6 also depicts possible gait transition of bipedal walking based on event-driven, which indicate that appropriate dynamics and variables are selected and applied according to the state. In the state that has ramification such as state (IV) in Fig.6 into state (IV′) or (V) or (VII), the gait is switched to next state in case that auxiliary switching condition written above the allow in the figure indicating phase transient is satisfied. In the gait transition from (VII′) or (VIII′) to (IX), supporting-foot is switched from one foot to the other foot with renumbering of link, joint and angle's number. What the authors want to emphasize here is that the varieties of this transition completely depend on the solution of dynamics.A condition that heel of supporting-foot detaches from the ground in Fig. 6 (I), (IV), (IV′), (VII) to (II), (V), (V′), (VIII) was discussed in [19]. Also, state (IV) shows the lifting leg has knee constraint in the air, and the state(VI) shows lifting leg has knee constraint when the heel of supporting foot detaches. When floating-foot attaches to ground, we need to consider heel/toe-strike motion. We assume that this heel/toe-strike can be represented by completely inelastic collision introduced in [7]. Figure 6 has two kinds of bumping concerning heel and toe. We denoted dynamics of bumping between the heel and the ground in [19].

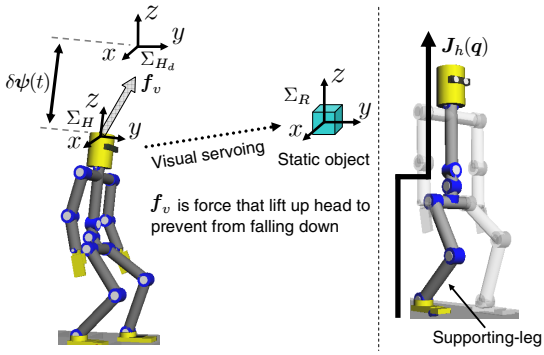

Fig. 7 Concept of Visual-Lifting Control

4. VISUAL-LIFTING APPROACH

4.1. Feedback Lifting Torque Generator

This section propose a vision-feedback control for improving humanoid's standing/walking stability as shown in Fig.7. We use a model-based matching method to measure pose of a static target object denoted by ${}^{H}\boldsymbol{\psi_R}(t)$ based on Σ_H, which represents the robot's head. The desired relative pose of Σ_R (reference target object's coordinate) and Σ_H is predefined by Homogeneous Transformation as ${}^{H}\boldsymbol{T}_R$. The difference of the desired head pose Σ_{H_d} and the current pose Σ_H is denoted as ${}^{H}\boldsymbol{T}_{H_d}$, it can be described by:

$$\begin{aligned} &{}^{H}\boldsymbol{T}_{H_d}({}^{H}\boldsymbol{\psi}_{Rd}(t), {}^{H}\boldsymbol{\psi}_R(t)) \\ &= {}^{H}\boldsymbol{T}_R({}^{H}\boldsymbol{\psi}_R(t)) \cdot {}^{H_d}\boldsymbol{T}_R{}^{-1}({}^{H}\boldsymbol{\psi}_{Rd}(t)) \end{aligned} \quad (4)$$

where, although ${}^{H}\boldsymbol{T}_R$ is calculated by ${}^{H}\boldsymbol{\psi}_R(t)$ that can measured by on-line visual pose estimation method [17], [18], we assume this parameter as being detected correctly in this paper. ${}^{H}\boldsymbol{\psi}_{Rd}(t)$ represents desired pose relation between Σ_H and Σ_R. Here, the force exerted on the head to minimize $\delta\boldsymbol{\psi}(t) = {}^{H}\boldsymbol{\psi}_{Rd}(t) - {}^{H}\boldsymbol{\psi}_R(t)$ calculated from ${}^{H}\boldsymbol{T}_{H_d}$—the pose deviation of the robot's head caused by gravity force and walking dynamical influences—is considered to be directly proportional to $\delta\boldsymbol{\psi}(t)$. The joint torque $\boldsymbol{\tau}_h(t)$ that pulls the robot's head up is given the following equation:

$$\boldsymbol{\tau}_h(t) = \boldsymbol{J}_h(\boldsymbol{q})^T \boldsymbol{K}_p \delta\boldsymbol{\psi}(t) \quad (5)$$

where $\boldsymbol{J}_h(\boldsymbol{q})$ in Fig. 7 is Jacobian matrix of the head pose against joint angles including $q_1, q_2, q_3, q_4, q_9, q_{10}, q_{11}, q_{18}$, and $\boldsymbol{K}_p$ means proportional gain similar to impedance control. We use this input to compensate the falling motions caused by gravity or dangerous slipping motion happened unpredictably during all walking states in Fig. 6. Notice that the input torque for non-holonomic joint like joint-1 (toe of supporting-foot), τ_{h_1} in $\boldsymbol{\tau}_h(t)$ in Eq. (4) is to be set as zero since it is free joint. Although $\delta\boldsymbol{\psi}(t)$ can represent error concerning the humanoid's both position and orientation, only position was utilized in this research, so $\boldsymbol{K}_p$ was set as $\boldsymbol{K}_p = diag[20, 290, 1100]^T$.

4.2. Feedforward leg and body motion generator

In addition to $\boldsymbol{\tau}_h(t)$, we used two input torques: $\boldsymbol{\tau}_t(t) = [0, \cdots, 0, \tau_{t5}, 0, \cdots, 0]^T$ to make floating-leg

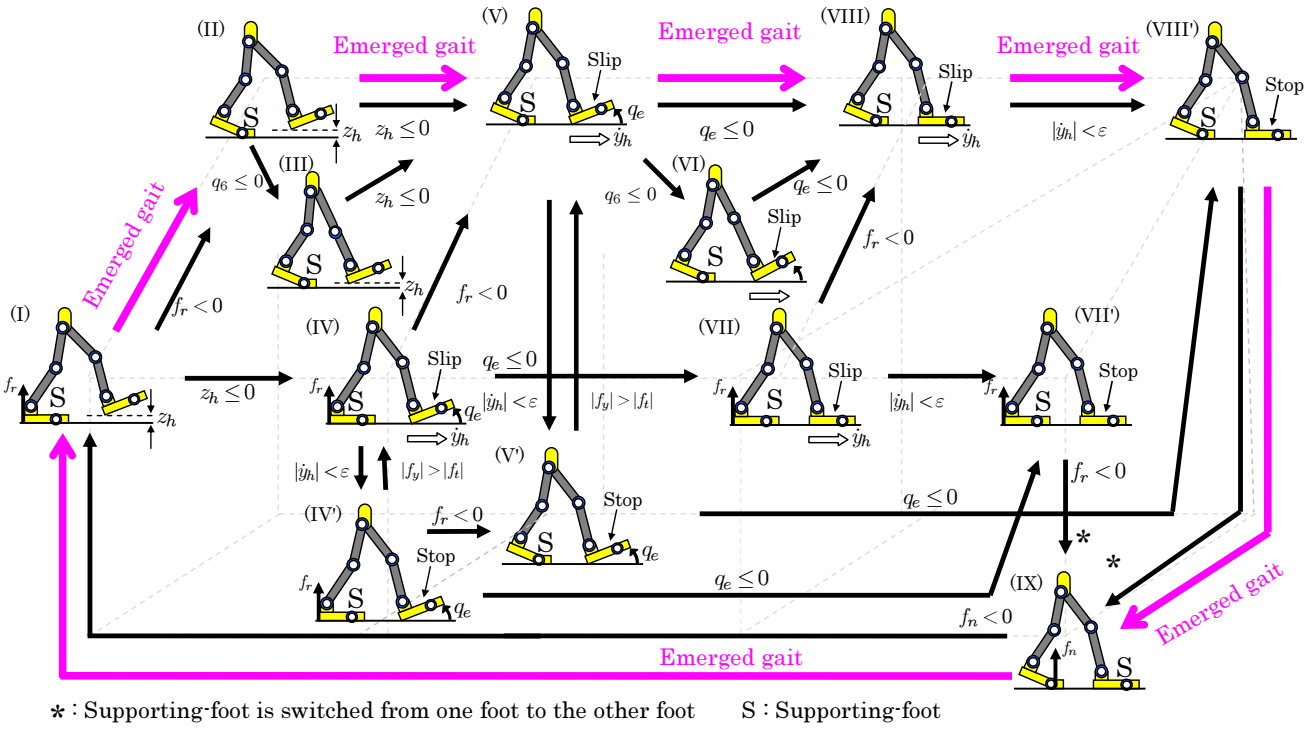

Fig. 6 State, gait's transition and emerged walking gait

(joint-5) step forward and $\boldsymbol{\tau}_w(t) = [0, \cdots, 0, \tau_{w11}, 0, \cdots, 0]^T$ to swing waist's roll angle (joint-11) according to supporting-foot. The element τ_{t5} and τ_{w11} of $\boldsymbol{\tau}_t(t)$ and $\boldsymbol{\tau}_w(t)$ are shown below:

$$\tau_{t5} = 20\cos\{2\pi(t - t_1)/1.85\}, \tag{6}$$

$$\tau_{w11} = \begin{cases} 50\sin\{2\pi(t - t_1)/1.85\} & (if\ \text{Right leg}) \\ -50\sin\{2\pi(t - t_1)/1.85\}\ (if\ \text{Left leg}). \end{cases} \tag{7}$$

Here, t_1 means the time that supporting-foot and contacting-foot are switched described in section IV and V.

4.3. Combined Lifting/Swinging Controller

Combining three torque generators expressed as Eqs. (4), (5) and (6), a controller for walking is created as $\boldsymbol{\tau}(t) = \boldsymbol{\tau}_h(t) + \boldsymbol{\tau}_t(t) + \boldsymbol{\tau}_w(t)$.

5. KNEE CONSTRAINT SIMULATION OF HUMANOID ROBOT

This time, we simulate knee constraint of humanoid robot. When the knee of the humanoid robot is fully extended in walking, knee joint angle of lifting leg is constrained as $q_6 = 0$[rad].

5.1. Controller to Knee Joint

Input torque τ_6 to knee was changed in order to constrain to knee during walking.

$$\tau_6 = \begin{cases} 60(t - t_2) & (t > 1.6) \\ 100(-0.4 - q[6])\ (t \le 1.6). \end{cases} \tag{8}$$

$$\tau_5 = \begin{cases} 25.0\cos(2.0\pi(t - t_2)/1.85)\ (t > 1.6) \\ 20.0\cos(2.0\pi(t - t_2)/1.85)\ (t \le 1.6). \end{cases} \tag{9}$$

t_2 is the switching time for supporting leg and lifting leg and t is current time. Also τ_5 and τ_6 represent the input torques to knee and hip joint angle. In order to stabilize the posture of walking immediately after the start, we changed the input torque at t=1.6[s]. For stretching the leg though knee, the stride should be lengthened. To this problem, stretching of knee joint is achieved by increasing the input torque to hip and knee joint of lifting leg.

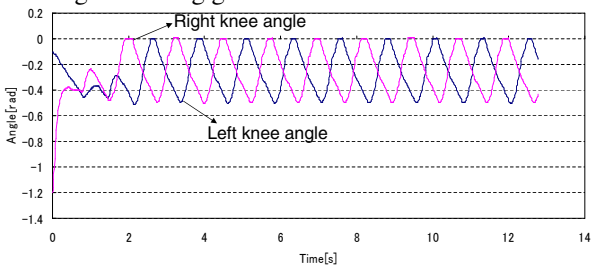

Fig. 8 Angular variation of the knee

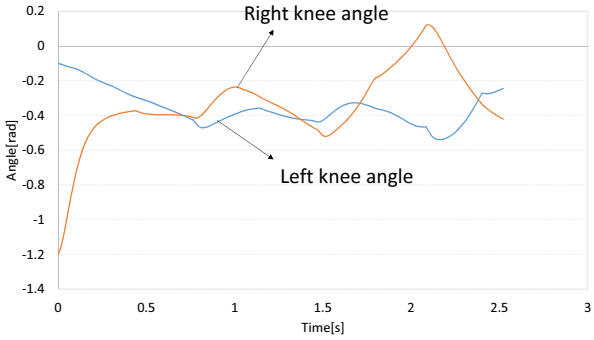

Fig. 9 Angular variation of the knee by no knee constraint

5.2. Knee Joint Angle is changed by Knee Constraint

Keeping the constraint condition, we examined the variation of the hip joint angle in walking. Fig.9 indicates

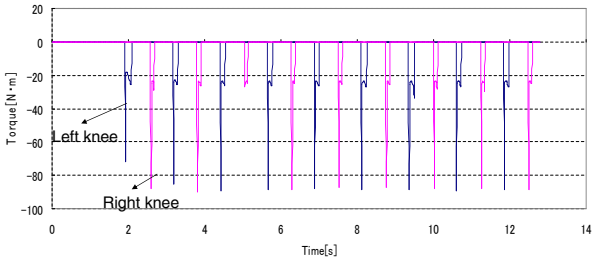

Fig. 10 Constraint torgue of the knee

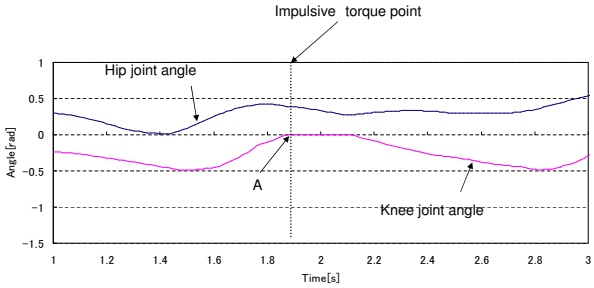

Fig. 11 Hip joint angle is changed by the impulsive torque

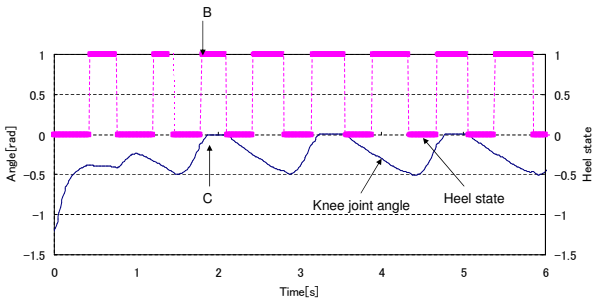

Fig. 12 Knee joint angle and heel state

that angle of knee joint is over 0[rad] by non-constraint simulation, it can't walk from 2.6 seconds. On the other hand Fig.8, it can find that the angle of knee joint does not exceed 0[rad]. And q_6=0 means the knee is straighted because the way of taking q_6 is indicated by Fig.1. Therefore, the simulation result show that the knee joint is constrained while walking.

5.3. Constraint Torque and Impulsive Force

Fig.10 shows that the value of the constraint torque to knee becomes large spikily, because the impact force is generated when knee is constrained that is collision.

5.4. Hip Joint Angle is Changed Before and After Collision

We consider that the impact force influences the walking and the increase of the angle of hip joint. But Fig.11 shows that the angle of hip joint does not increase before and after the collision as indicated by A. In this cause, we thought that it was caused by grounding of lifting leg before the knee constraining happens. So we examined the grounding time of lifting leg before constraining the knee and showed their results in Fig.12. "Heel state" in the figure means that lifting leg is in the air when Heel state=0, and the lifting leg is contacting with floor it is 1. Fig.12 shows the knee is constrained after the lifting leg is

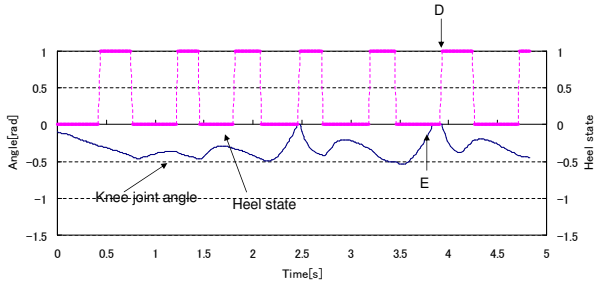

Fig. 13 Knee joint angle and heel state(New walking)

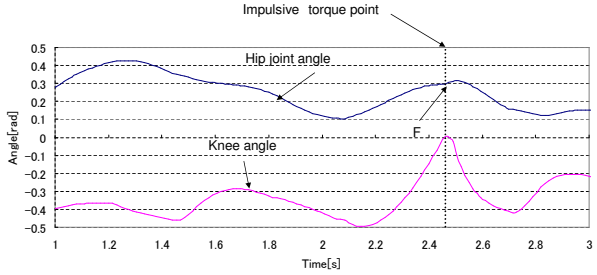

Fig. 14 Hip joint angle by impulsive torque

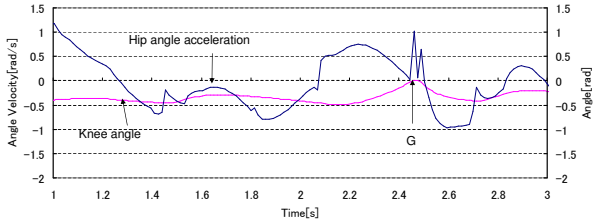

Fig. 15 Hip joint angle and angular velocity by the impulsive torque

contacting with floor as indicated by B and C. This is the reason why the hip joint angle does not increase. So we have to make the controller that can make the leg ground after constraining the knee for improving the walking.

5.5. Controller is Changed

$$\tau_6 = \begin{cases} 60(t - t_2)) & (t > 1.6) \\ 100(-0.4 - q[6]) \ (t \leq 1.6). \\ -200(t - t_2) \ (if \ knee \ is \ constrained) \end{cases} \quad (10)$$

$$\alpha = \begin{cases} 1.0 \ (t > 1.6) \\ 1.2 \ (t \leq 1.6). \end{cases} \quad (11)$$

In this time we have changed the controller in two points. The first point is to increase the value of weighting factor α for Visual-lifting Approach. This point can make the period of walking longer, and the tidemark of foot higher. The second point is to introduce the torque for turning the leg in order to ground the leg with keeping knee constraint. In this point, we gave the input torque to knee joint for grounding the lifting leg with bending the knee again after stretching the knee, because the lifting leg cannot change from point contacting to surface contacting with keeping the state of knee constraint.

5.6. Hip Joint Angle and Angular Velocity is Increased

In the new walking, we examined the grounding time of lifting leg before constraining the knee again and

showed their results in Fig.13. Fig.13 shows that the knee is constrained before lifting leg is contacting with floor as indicated by D and E. Fig.14 shows that the angle of hip joint increased after the collision as indicated by F. Fig.15 shows that the angle velocity also increased immediately after the collision as indicated by G. From these results, we can estimate that the impact force influences the humanoid robot's walking, and the length of stride is influenced by the angle of hip joint. However, this walking achieves only four steps. As future work, we aim for long-distance walking of humanoid robot through our approach.

6. CONCLUSION

In this paper, the humanoid robot's walking simulation with knee constraint shows the increase of the angle and the angular velocity of knee joint and it found that the impact force influenced the walking. Although Visual-lifting Approach is effective for knee constraint, further improvement of our approach is needed because the simulation of this paper achieves only four steps. As future works, we validate the effectiveness of Visual-lifting Approach through actual equipment considering the impact force.

REFERENCES

[1] M. Vukobratovic, A. Frank and D. Juricic, "On the Stability of Biped Locomotion," *IEEE Transactions on Biomedical Engineering*, Vol.17, No.1, 1970.

[2] M. Vukobratovic and J. Stepanenko, "On the Stability of Anthropomorphic Systems," *Mathematical Biosciences*, Vol.15, pp.1–37, 1972.

[3] S. Colins, A. Ruina, R. Tedrake and M. Wisse, "Efficient Bipedal Robots Based on Passive-Dynamic Walkers," *Science*, Vol.307, pp.1082–1085, 2005.

[4] J. Pratt, P. Dilworth and G. Pratt, "Virtual Model Control of a Bipedal Walking Robot," *Proceedings of IEEE International Conference on Robotics and Automation*", pp.193–198, 1997.

[5] R.E. Westervelt, W.J. Grizzle and E.D. Koditschek, "Hybrid Zero Dynamics of Planar Biped Walkers," *IEEE Transactions on Automatic Control*, Vol.48, No.1, pp.42–56, 2003.

[6] Y. Harada, J. Takahashi, D. Nenchev and D. Sato, "Limit Cycle Based Walk of a Powered 7DOF 3D Biped with Flat Feet," *Proceedings of IEEE/RSJ International Conference on Intelligent Robots and Systems*, pp.3623–3628, 2010.

[7] Y. Huang, B. Chen, Q. Wang, K. Wei and L. Wang, "Energetic efficiency and stability of dynamic bipedal walking gaits with different step lengths," *Proceedings of IEEE/RSJ International Conference on Intelligent Robots and Systems*, pp.4077–4082, 2010.

[8] T. Wu, T. Yeh and B. Hsu, "Trajectory Planning of a One-Legged Robot Performing Stable Hop," *Proceedings of IEEE/RSJ International Conference on Intelligent Robots and Systems*, pp.4922–4927, 2010.

[9] Y. Nakamura and K. Yamane, "Dynamics of Kinematic Chains with Discontinuous Changes of Constraints—Application to Human Figures that Move in Contact with the Environments—," *Journal of RSJ*, Vol.18, No.3, pp.435–443, 2000 (in Japanese).

[10] K.Yamane and Y.Nakamura, "Dynamics Filter - Concept and Implementation of On-Line Motion Generator for Human Figures," IEEE Transactions on Robotics and Automation, vol.19, No.3, pp.421-432, 2003.

[11] M. Kouchi, M. Mochimaru, H. Iwasawa and S. Mitani, "Anthropometric database for Japanese Population 1997-98," Japanese Industrial Standards Center (AIST, MITI), 2000.

[12] Y. Fujimoto and A. Kawamura, "Three Dimensional Digital Simulation and Autonomous Walking Control for Eight-Axis Biped Robot," *Proceedings of IEEE International Conference on Robotics and Automation*, pp.2877–2884, 1995.

[13] J.Y.S. Luh, M.W. Walker and R.P.C. Paul, "On-Line Computational Scheme for Mechanical Manipulators," *ASME Journal of Dynamics Systems, Measurement, and Control*, Vol.102, No.2, pp.69–76, 1980.

[14] M.W. Walker and D.E. Orin, "Efficient Dynamic Computer Simulation of Robotic Mechanisms," *ASME Journal of Dynamics Systems, Measurement, and Control*, Vol.104, pp.205–211, 1982.

[15] T. Mita and K. Osuka, "Introduction to Robot Control," CORONA PUBLISHING CO., LTD., 1989 (in Japanese).

[16] N. Hogan, "Impedance Control; An Approach to Manipulation, Parts I–III, *ASME Journal of Dynamics Systems, Measurement, and Control* Vol.107, No.1, pp.1–24, 1985.

[17] W. Song, M. Minami, F. Yu, Y. Zhang and A. Yanou, "3-D Hand & Eye-Vergence Approaching Visual Servoing with Lyapunov-Stable Pose Tracking," *Proceedings of IEEE International Conference on Robotics and Automation*, pp.5210–5217, 2011.

[18] F. Yu, W. Song and M. Minami, "Visual Servoing with Quick Eye-Vergence to Enhance Trackability and Stability," *Proceedings of IEEE/RSJ International Conference on Intelligent Robots and Systems*, pp.6228–6233, 2010.

[19] T. Maeba, M. Minami, A. Yanou and J. Nishiguchi: "Dynamical Analyses of Humanoid's Walking by Visual Lifting Stabilization Based on Event-driven State Transition", 2012 IEEE/ASME Int. Conf. on Advanced Intelligent Mechatronics Proc., pp.7-14, 2012.